Supplementary Information for

Lipid synthesis, triggered by PPARγ T166 dephosphorylation, sustains reparative function of macrophages during tissue repair

Shiman Zuo[1#], Yuxin Wang[1#], Hanjing Bao[1], Zehui Zhang[1], Nanfei Yang[1], Meng Jia[1], Qing Zhang[2], Ani Jian[1], Rong Ji[3], Lidan Zhang[3], Yan Lu[1], Yahong Huang[1], Pingping Shen[1,4]*

[1]State Key Laboratory of Pharmaceutical Biotechnology and Department of Urology, Nanjing Drum Tower Hospital, The Affiliated Hospital of Nanjing University Medical School, School of Life Sciences, Nanjing University, Nanjing 210023, China.

[2]Department of Urology, Drum Tower Hospital, Medical School of Nanjing University, Institute of Urology, Nanjing University, Nanjing 210008, China.

[3]State Key Laboratory of Pollution Control and Resource Reuse, School of The Environment, Nanjing University, Nanjing 210023, China.

[4]Shenzhen Research Institute of Nanjing University, Shenzhen 518000, China.

# Equally Contributing Authors.

* Corresponding author.

E-mail address: ppshen@nju.edu.cn (P. Shen)

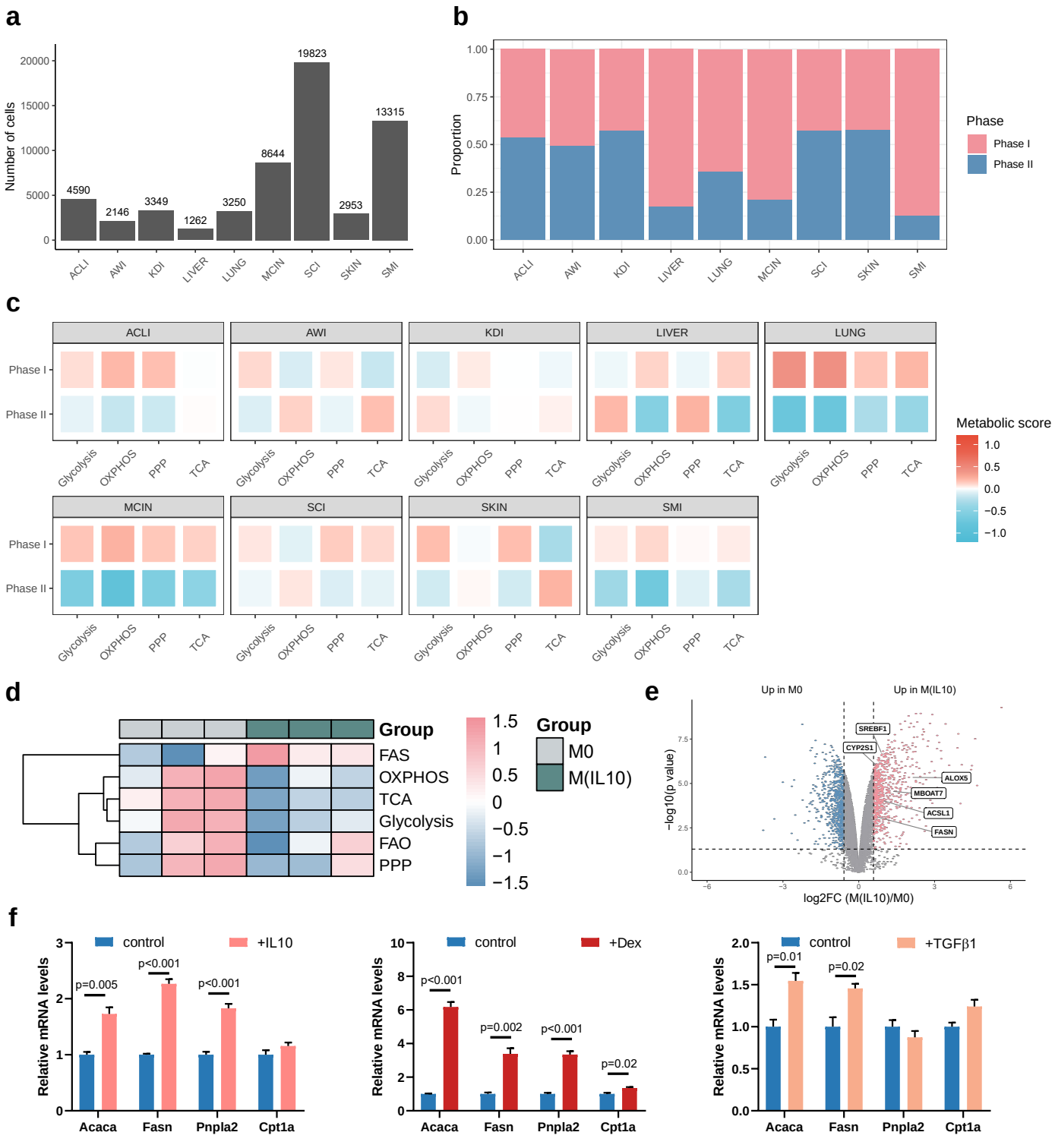

Supplementary Fig. 1 Metabolic profiles of injury-associated macrophages. **a** Bar plot showing the number of macrophages collected in each tissue healing model. **b** The fraction of cells originating from the 2 phases across multiple wound healing models. **c** Heatmaps showing different expression patterns of glycolysis-, OXPHOS-, PPP-, and TCA-associated signature genes between phase I and phase II macrophages. **d** Heatmaps showing different expression patterns of FAS-, FAO-, glycolysis-, OXPHOS-, PPP-, and TCA-associated signature genes among polarized human monocyte-derived macrophages of GSE162698 dataset. **e** Volcano plot showing specifically upregulated genes in human BMDMs upon IL-10 treatment vs control. Differential genes enriched in M0 or M(IL10) are represented in blue and pink, respectively (n = 3 biological replicates per group). **f** mRNA expression of lipid metabolism genes in BMDMs stimulated with IL-10 (20 ng/ml, 48 h), dexamethasone (Dex; 100nM, 48 h) or TGF-β1 (20 ng/ml, 48 h) (n = 3 biological replicates per group). Data were analysed by a two-tailed Student's *t*-test.

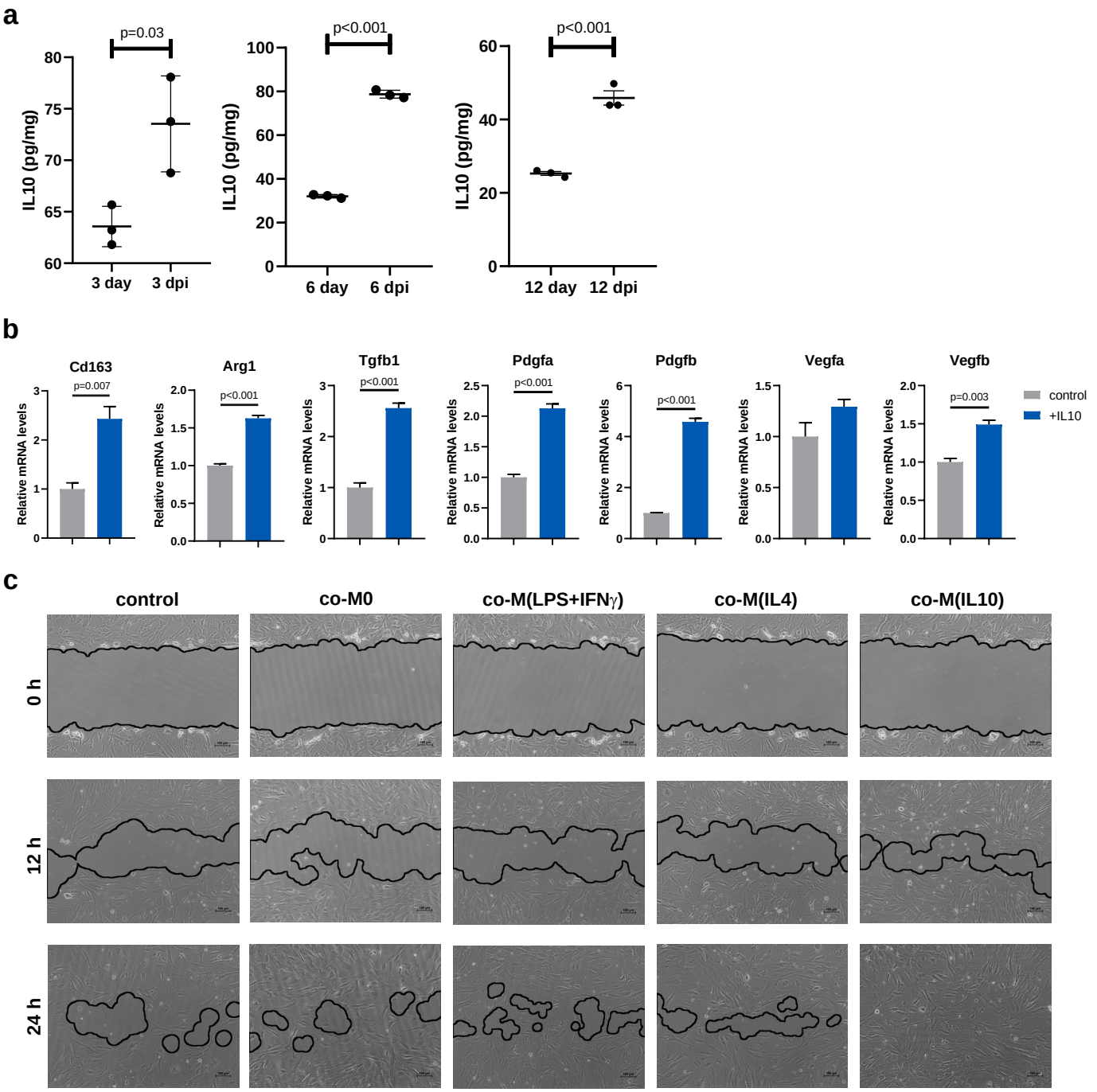

Supplementary Fig. 2 IL-10 induces reparative phenotype of macrophage in vitro. **a** The concentration of IL-10 in wound skin is determined by ELISA at indicated time points (*n* = 3). Data were analysed by a two-tailed Student's *t*-test. **b** mRNA expression of repair-associated genes in macrophages stimulated with IL-10 for 48 h. Data were analysed by a two-tailed Student's t-test and were presented as mean ± s.e.m. of *n* = 3 mice per group. **c** The scratch wound representative images of DFs co-cultured with M0, M(LPS+IFNγ), M(IL4) or M(IL10) BMDMs for 24 h.

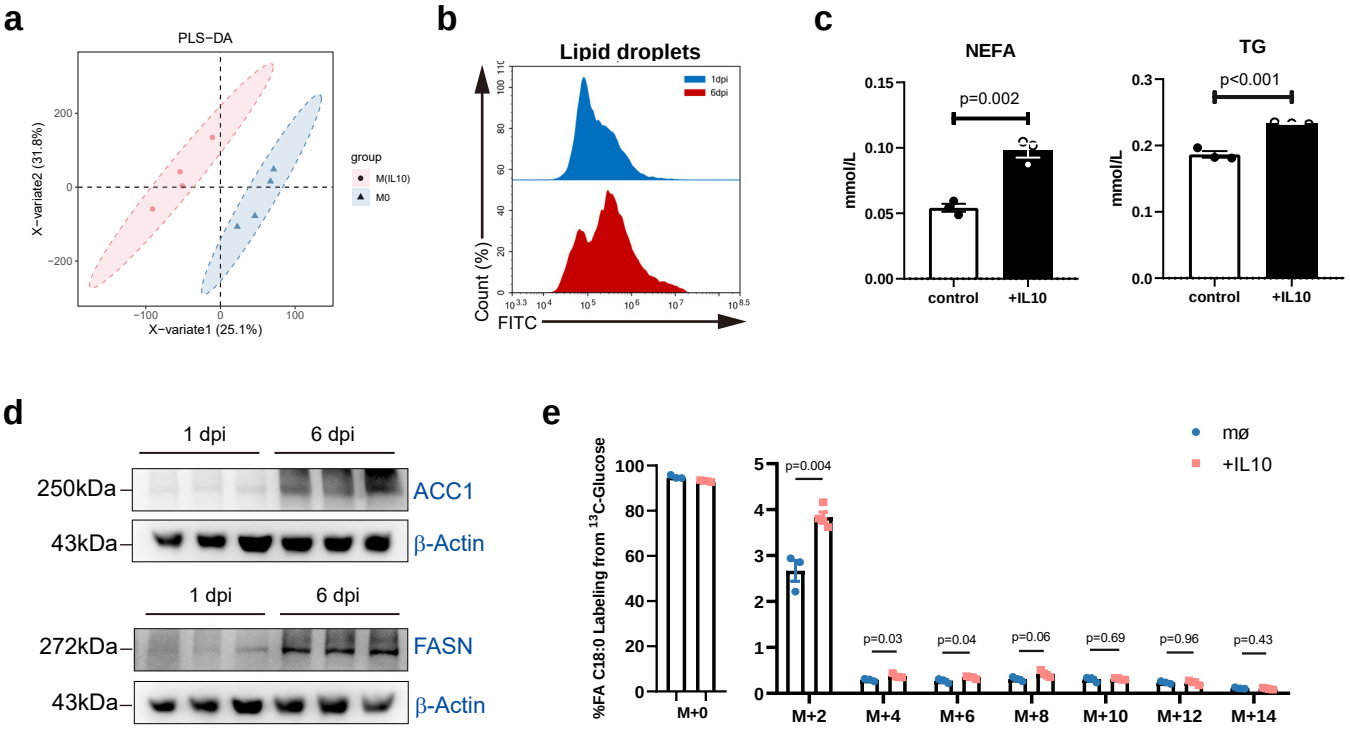

Supplementary Fig. 3 Evidence for increased lipid synthesis in reparative macrophages. **a** Partial Least-Squares Discriminant Analysis (PLS-DA) of lipidomic profiles of M(IL10) and M0. **b** BODIPY 493/503 staining analysis by flow cytometry in 1dpi and 6dpi wound macrophages. **c** NEFA and TGs content of BMDMs in response to IL-10. Data is presented as mean ± s.e.m. of *n* = 3 biological replicates. Data were analysed by a two-tailed Student's *t*-test. **d** ACC1 and FASN protein expression in MACS-sorted skin macrophages (F4/80^{+}) from 1 dpi and 6 dpi mice. Representative western blot analysis of *n* = 3 biological replicates. β-actin was used as the loading control. **e** The percentages of various isotopomers of FA 18:0 after trace to [U-^{13}C] glucose in BMDMs in the presence or absence of IL-10. Data were analysed using unpaired two-tailed Student's *t*-test. Values are mean ± s.e.m. *n* = 3 (control) and *n* = 4 (IL-10) biologically independent samples.

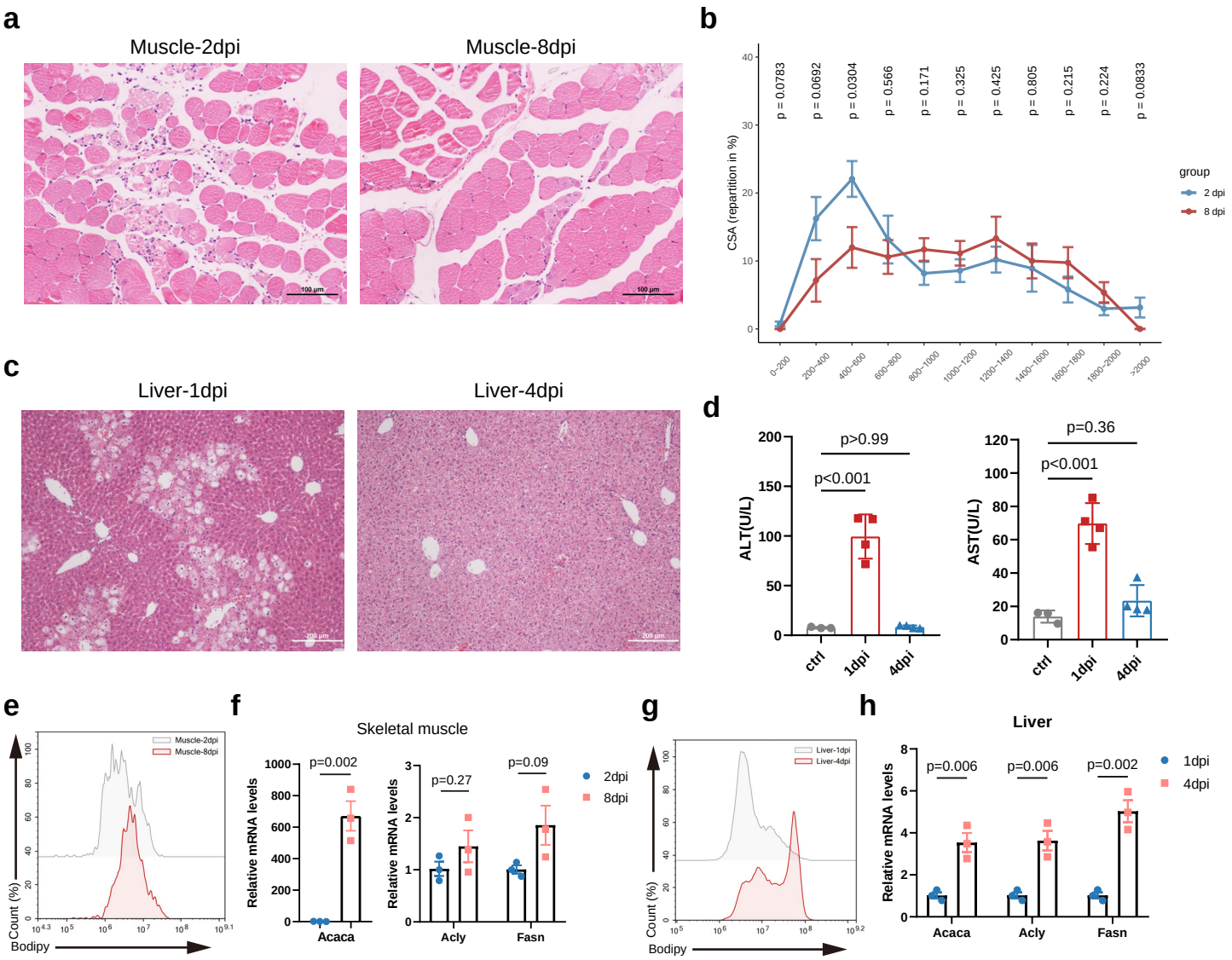

Supplementary Fig. 4 Fatty acid synthesis increased in macrophages during the reparative phase in muscle injury and liver injury models. **a** Representative H&E images of 2 dpi and 8 dpi muscle sections. Scale bar, 100 μm. **b** Repartition of fiber cross section area (CSA) at 2 dpi and 8 dpi. Data indicated mean ± s.e.m. of *n* = 6 biological replicates. Data were analysed by a two-tailed Student's *t*-test. **c** Representative H&E images of 1 dpi and 4 dpi liver sections. Scale bar, 200 μm. **d** Serum ALT and AST levels in control (*n* = 3), 2 dpi and 8 dpi mice. Data is presented as mean ± s.e.m. of *n* = 4 biological replicates. Data were analysed by a one-way ANOVA followed by a Dunnett's multiple-comparisons test. **e** BODIPY 493/503 staining analysis by flow cytometry in MACS-sorted muscle macrophages (F4/80$^+$) from 2 dpi and 8 dpi mice. **f** Relative mRNA levels of lipid synthesis-related genes in MACS-sorted muscle macrophages (F4/80$^+$) from 2 dpi and 8 dpi mice. *n* = 3 biologically independent mice per group. Data were analysed by a two-tailed Student's *t*-test. **g** BODIPY 493/503 staining analysis by flow cytometry in MACS-sorted liver macrophages (F4/80$^+$) from 1 dpi and 4 dpi mice. **h** Relative mRNA levels of lipid synthesis-related genes in MACS-sorted liver macrophages (F4/80$^+$) from 1 dpi and 4 dpi mice. *n* = 3 biologically independent mice per group. Data were analysed by a two-tailed Student's *t*-test.

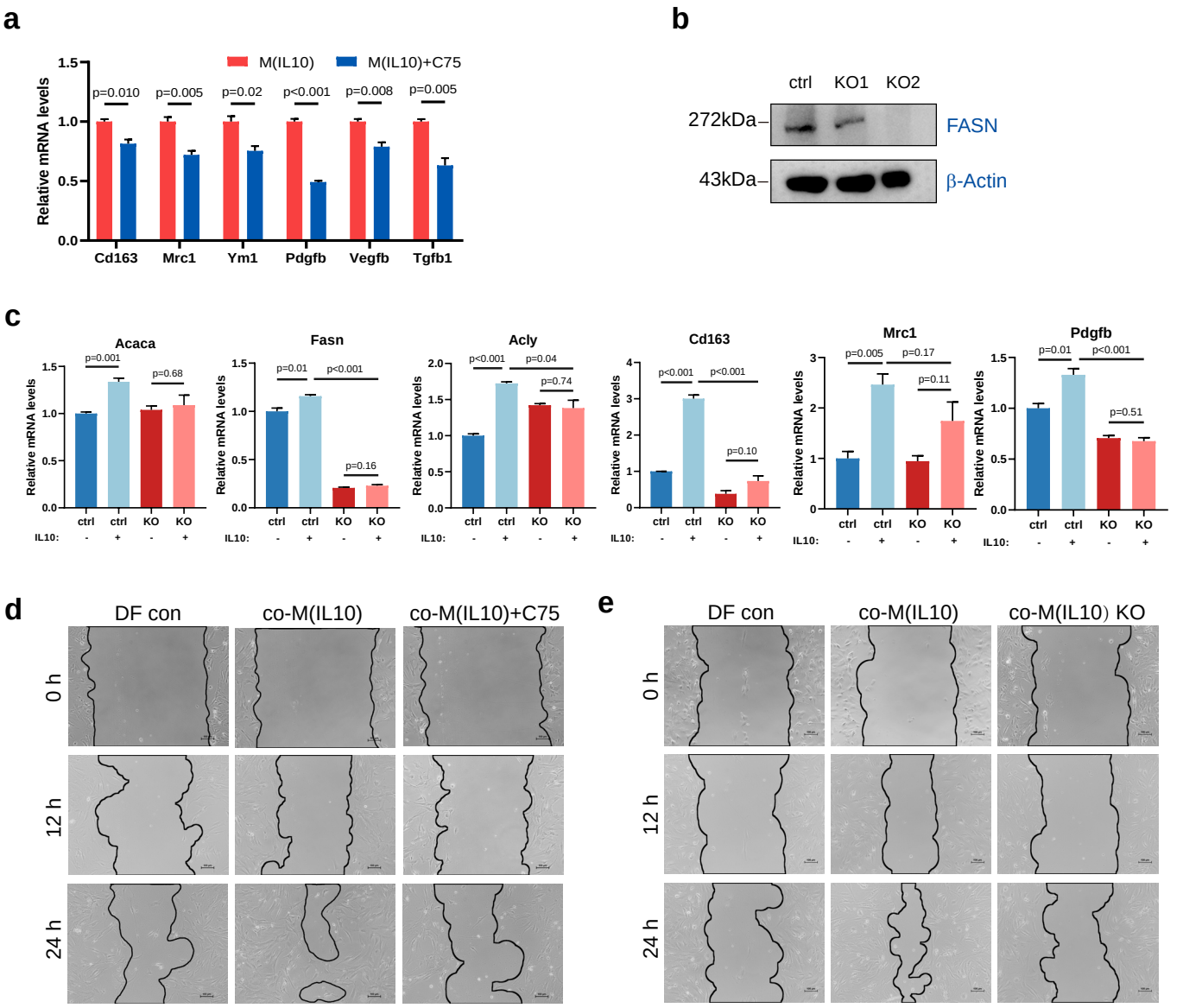

Supplementary Fig. 5 Lipid synthesis is required for the activation and function of reparative macrophages. **a** Relative mRNA levels of macrophages repair-associated genes in vehicle (DMSO) or C75-treated BMDMs in response to IL-10, *n* = 3 biological replicates per group. Data were analysed by a two-tailed Student's *t*-test. **b** Western blotting analysis of FASN expression in FASN-knockout (KO) RAW264.7 macrophages. **c** Expression of the fatty acid synthesis genes and reparative markers in FASN-KO cells in response to IL-10. mRNA amounts normalized relative to *Rplp0* (*n* = 3). Data were analysed by a two-tailed Student's *t*-test. **d** The scratch wound representative images of DFs co-cultured with M(IL10) or treatment with C75 for 24 h. **e** The scratch wound representative images of DFs co-cultured with M(IL10) or M(IL10) KO FASN for 24 h.

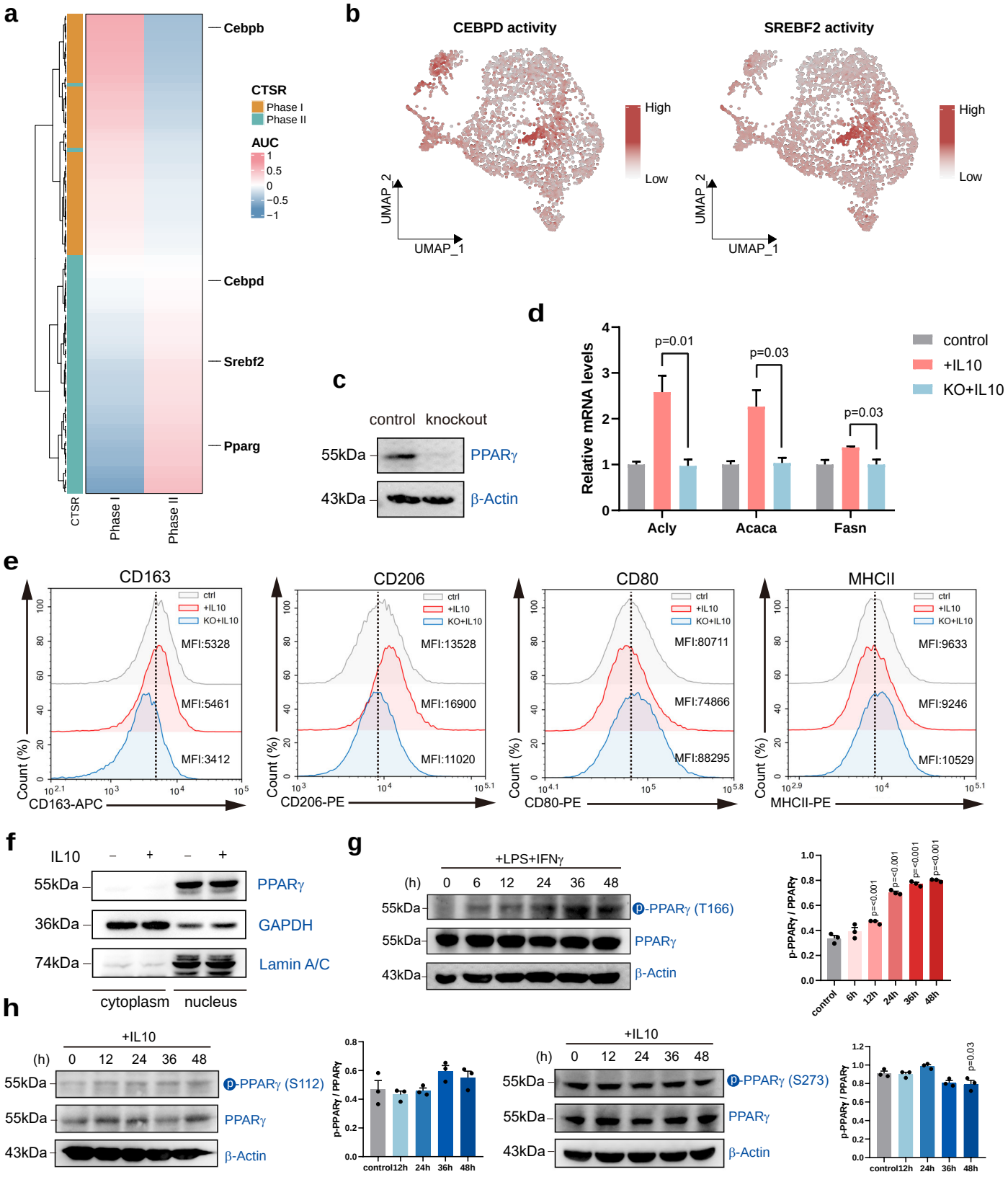

Supplementary Fig. 6 PPARγ is a key transcription factor regulating lipid metabolism in reparative macrophages. **a** SCENIC analysis of transcription factor activities of phase I and phase II wound macrophages. **b** UMAP plots showing the activity of indicated transcription factors in macrophages from skin wound healing phase I and phase II. **c** Western blotting analysis of PPARγ expression in PPARγ-knockout cells. **d** The relative mRNA levels of fatty acid synthesis-related genes in control or KO-PPARγ RAW 264.7 cells were assessed by RT-qPCR after treatment with IL-10 for 48 h. Data were analysed by a two-tailed Student's *t*-test. **e** CD163, CD206, CD80 and MHCII levels of control or KO-PPARγ RAW 264.7 cells were measured by flow cytometric after treatment with IL-10 for 48 h. **f** Immunoblot analysis of PPARγ protein in cytoplasmic and nucleus fractions of BMDMs treated with or without IL-10. Lamin A/C and GAPDH were used as a nucleus and cytoplasmic normalization control, respectively. **g** Representative immunoblot of pPPARγT166 and total PPARγ in BMDMs treated with LPS+IFNγ. β-actin was used as a loading control. Data were analysed by a one-way ANOVA followed by a Dunnett's multiple-comparisons test. **h** Representative immunoblot of phospho-Ser112-PPARγ (pPPARγS112), phospho-Ser273-PPARγ (pPPARγS273) and total PPARγ in BMDMs treated with IL-10. β-actin was used as a loading control.

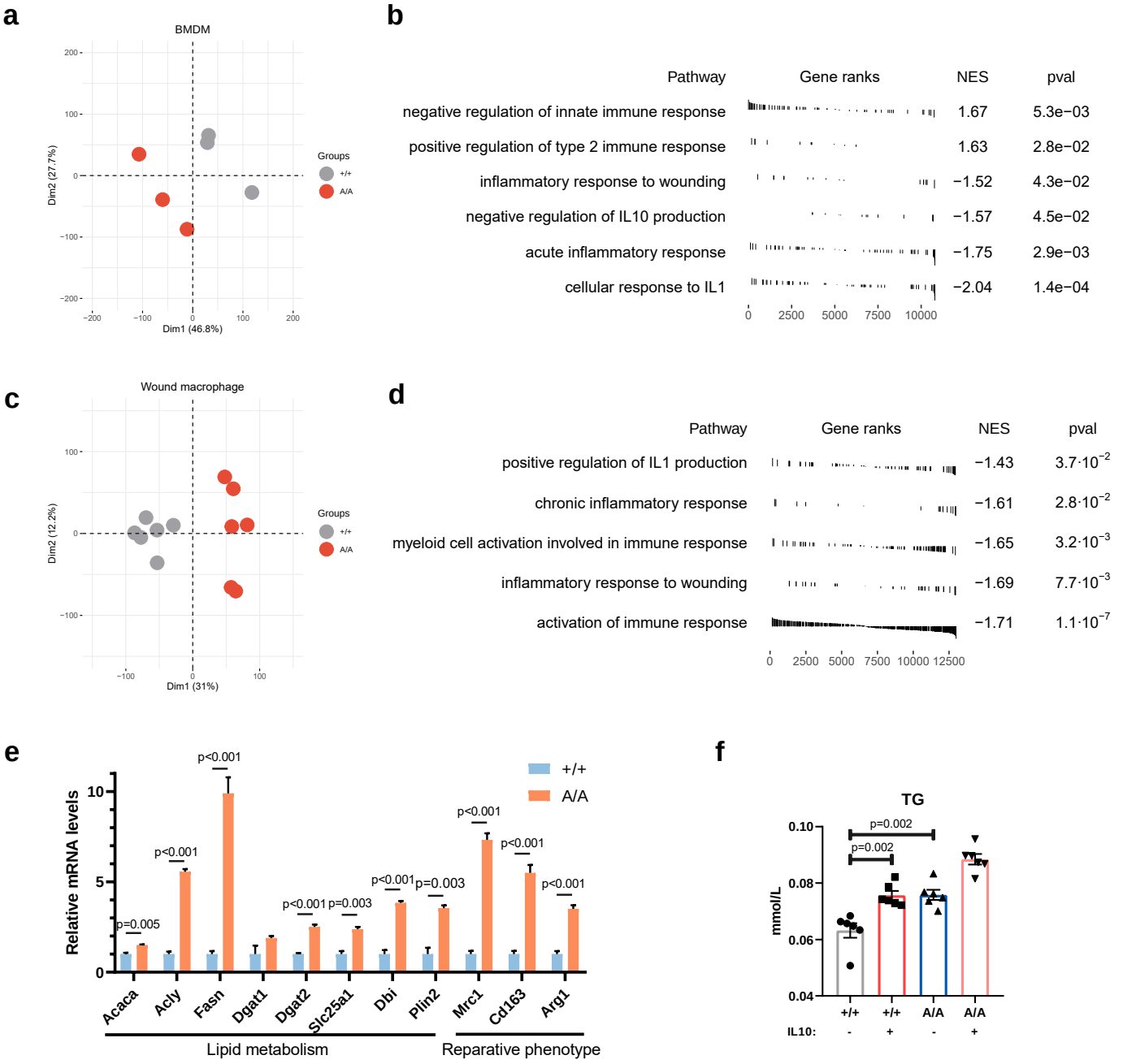

Supplementary Fig. 7 PPARγ T166 dephosphorylation regulates reparative phenotype of skin macrophages by controlling lipid metabolism. **a** Principal-component analysis (PCA) of RNA-seq data from PPARγ$^{+/+}$ and PPARγ$^{A/A}$ BMDMs with 3 biological replicates. **b** GSEA analysis showing the enrichment of indicated GO terms between PPARγ$^{+/+}$ and PPARγ$^{A/A}$ BMDMs. Genes were ranked by log2FC in the comparison of PPARγ$^{A/A}$ against PPARγ$^{+/+}$ samples. **c** PCA of RNA-seq data from PPARγ$^{+/+}$ and PPARγ$^{A/A}$ 6 dpi wound macrophages with 6 biological replicates. **d** GSEA analysis showing the enrichment of indicated GO terms between PPARγ$^{+/+}$ and PPARγ$^{A/A}$ 6 dpi wound macrophages. Genes were ranked by log2FC in the comparison of PPARγ$^{A/A}$ against PPAR γ$^{+/+}$ samples. **e** Relative mRNA levels of lipid metabolism genes and reparative markers in sorted wound macrophages (6 dpi) from PPARγ$^{+/+}$ and PPARγ$^{A/A}$ mice, *n* = 3 biologically independent mice per group. Data were analysed by a two-tailed Student's *t*-test. **f** TGs content of PPARγ$^{+/+}$ and PPARγ$^{A/A}$ BMDMs in response to IL-10. Data is presented as mean ± s.e.m. of *n* = 6 biological replicates. Data were analysed by a two-tailed Student's *t*-test.

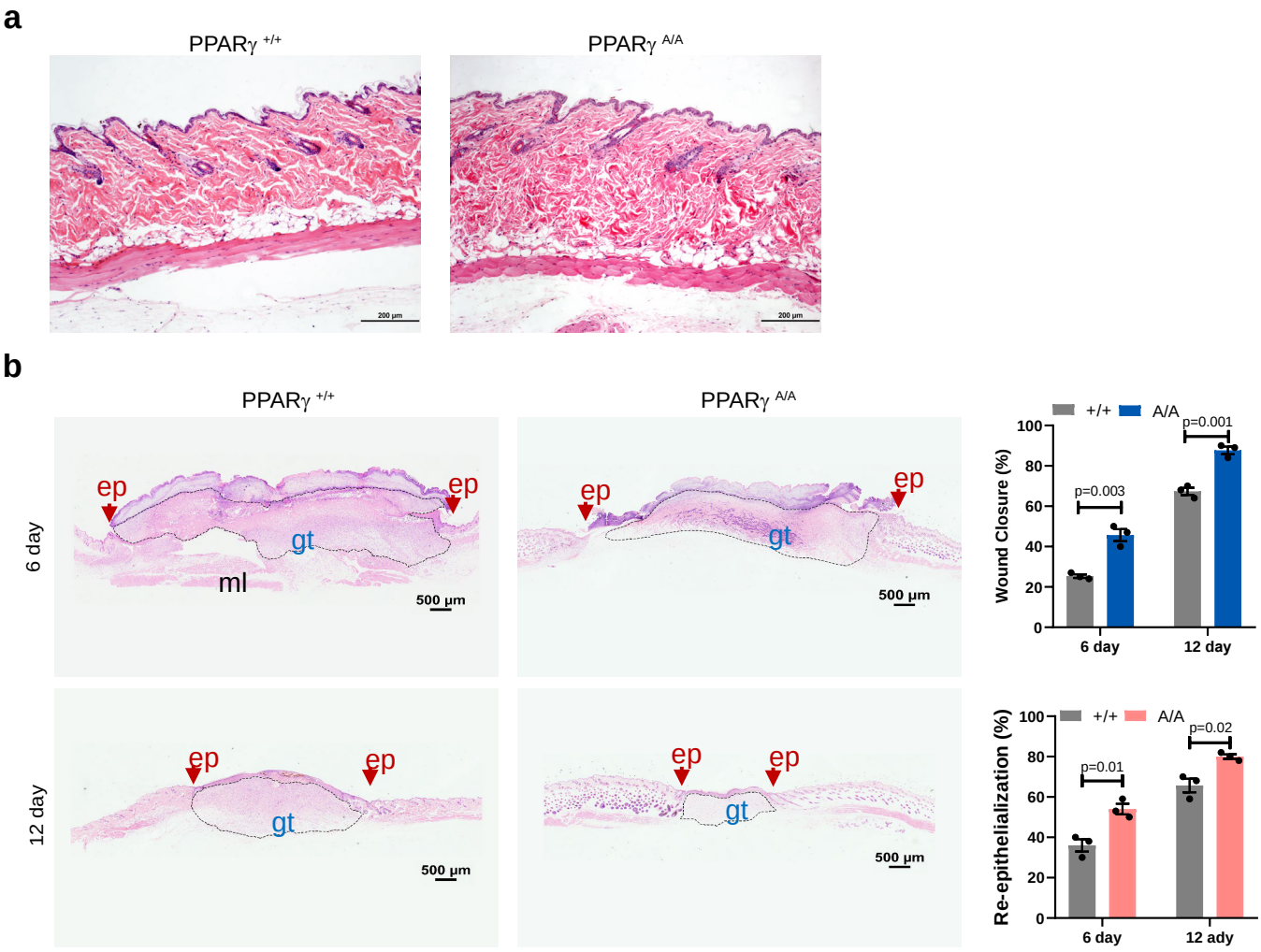

Supplementary Fig. 8 Blocking PPARγ T166 phosphorylation accelerates wound healing. **a** H&E staining of skin from 2-month-old PPARγ$^{+/+}$ and PPARγ$^{A/A}$ mice. **b** Representative H&E images of 6 and 12 dpi wound sections from PPARγ$^{+/+}$ (*n* = 3) and PPARγ$^{A/A}$ (*n* = 4) mice, and quantitative analysis of wound closure and re-epithelialization. Scale bar, 500 μm. Data were analysed by a two-tailed Student's *t*-test.

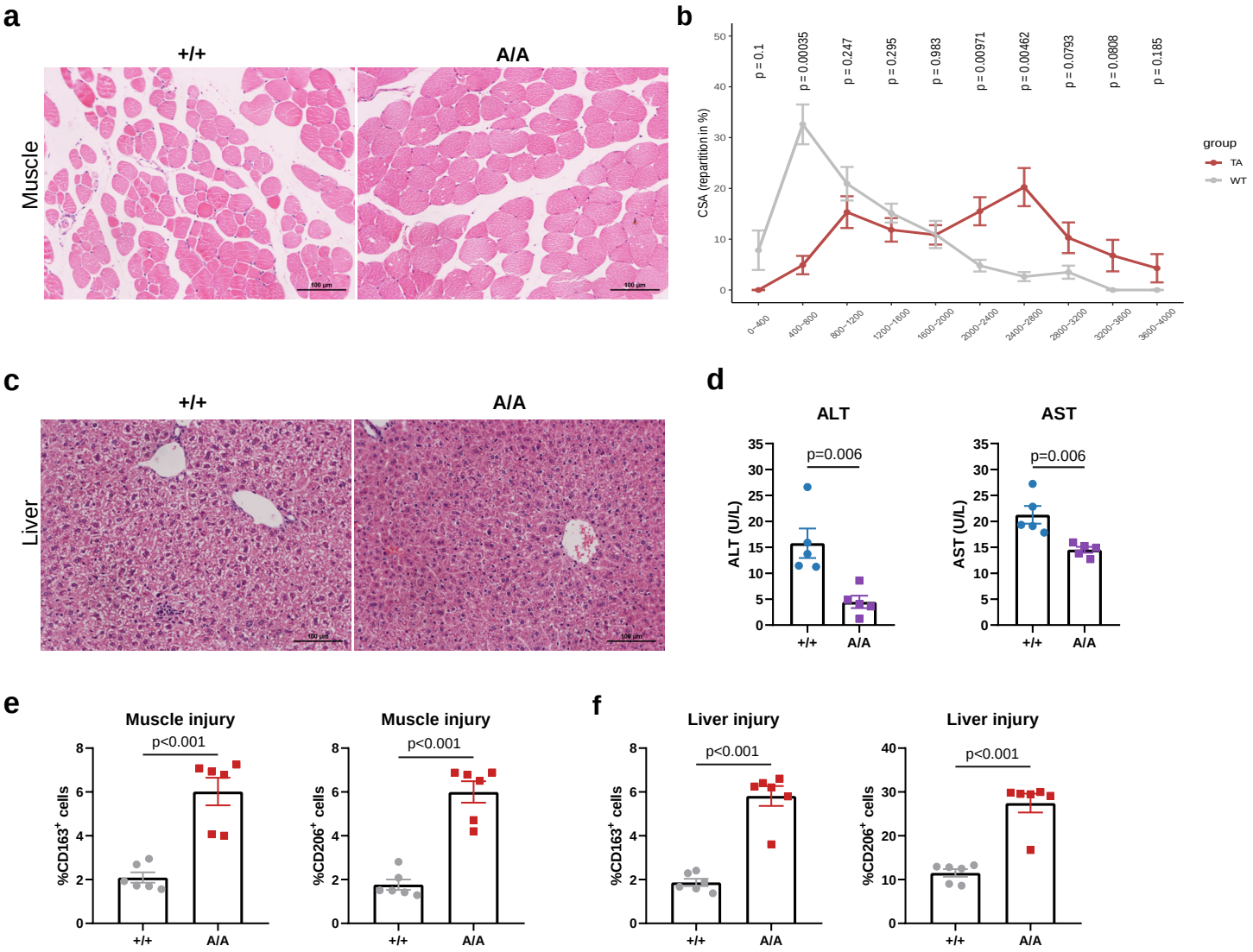

Supplementary Fig. 9 Dephosphorylation of PPARγ T166 improves muscle and liver tissue repair. **a** Representative H&E images of 8 dpi muscle sections from PPARγ$^{+/+}$ and PPARγ$^{A/A}$ mice. Scale bar, 100 µm. **b** Repartition of fiber CSA in PPARγ$^{+/+}$ and PPARγ$^{A/A}$ mice at 8 dpi. Data indicated mean ± s.e.m. of *n* = 6 biological replicates. Data were analysed by a two-tailed Student's *t*-test. **c** Representative H&E images of 4 dpi liver sections from PPARγ$^{+/+}$ and PPARγ$^{A/A}$ mice. Scale bar, 100 µm. **d** Serum ALT and AST levels in PPARγ$^{+/+}$ and PPARγ$^{A/A}$ mice at 4 dpi. Data is presented as mean ± s.e.m. of *n* = 5 biological replicates. Data were analysed by a two-tailed Student's *t*-test. **e** Expression of the CD163 and CD206 in 8 dpi muscle from PPARγ$^{+/+}$ and PPARγ$^{A/A}$ mice were assessed by flow cytometry. The quantification of percentage of CD163+ and CD206+ macrophages from *n* = 6 biological replicates is presented as mean ± s.e.m. Data were analysed by a two-tailed Student's *t*-test. **f** Expression of the CD163 and CD206 in 4 dpi liver from PPARγ$^{+/+}$ and PPARγ$^{A/A}$ mice were assessed by flow cytometry. The quantification of percentage of CD163^{+} and CD206^{+} macrophages from *n* = 6 biological replicates is presented as mean ± s.e.m. Data were analysed by a two-tailed Student's *t*-test.

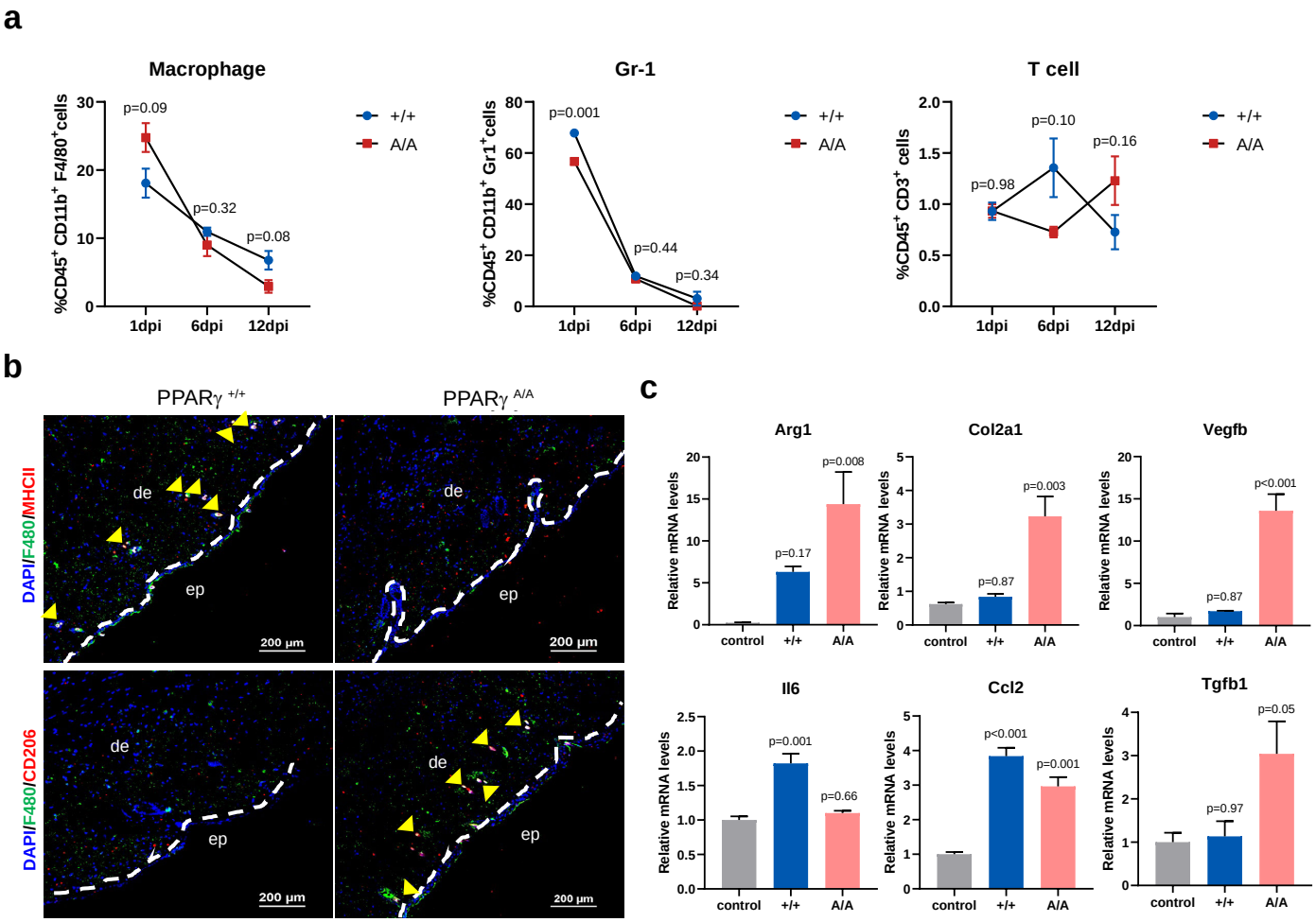

Supplementary Fig. 10 Characteristics of immune microenvironment in PPARγ$^{A/A}$ mice during skin regeneration. **a** Percentage of F4/80$^+$ macrophages, Gr1$^+$ granulocytes and CD3$^+$ T cells in the skins of 1, 6 and 12 dpi in PPARγ$^{+/+}$ and PPARγ$^{A/A}$ mice within the CD45$^+$ immune cell population. *n* = 3 biological replicates per group. **b** Immunofluorescent staining for F4/80 (green), CD206 (red), MHCII (red) and nuclei (blue) in 6 dpi wound sections from PPARγ$^{+/+}$ and PPARγ$^{A/A}$ mice. Scale bar, 200 µm. Dotted lines indicate the murine epidermis. Arrows indicate the CD206$^+$ or MHCII$^+$ macrophages. **c** Relative mRNA levels of pro-inflammatory and pro-repair associated genes at 6-dpi from PPARγ$^{+/+}$ and PPARγ$^{A/A}$ mice, *n* = 3 biological replicates per group. Data were analysed by a one-way ANOVA followed by a Dunnett's multiple-comparisons test.

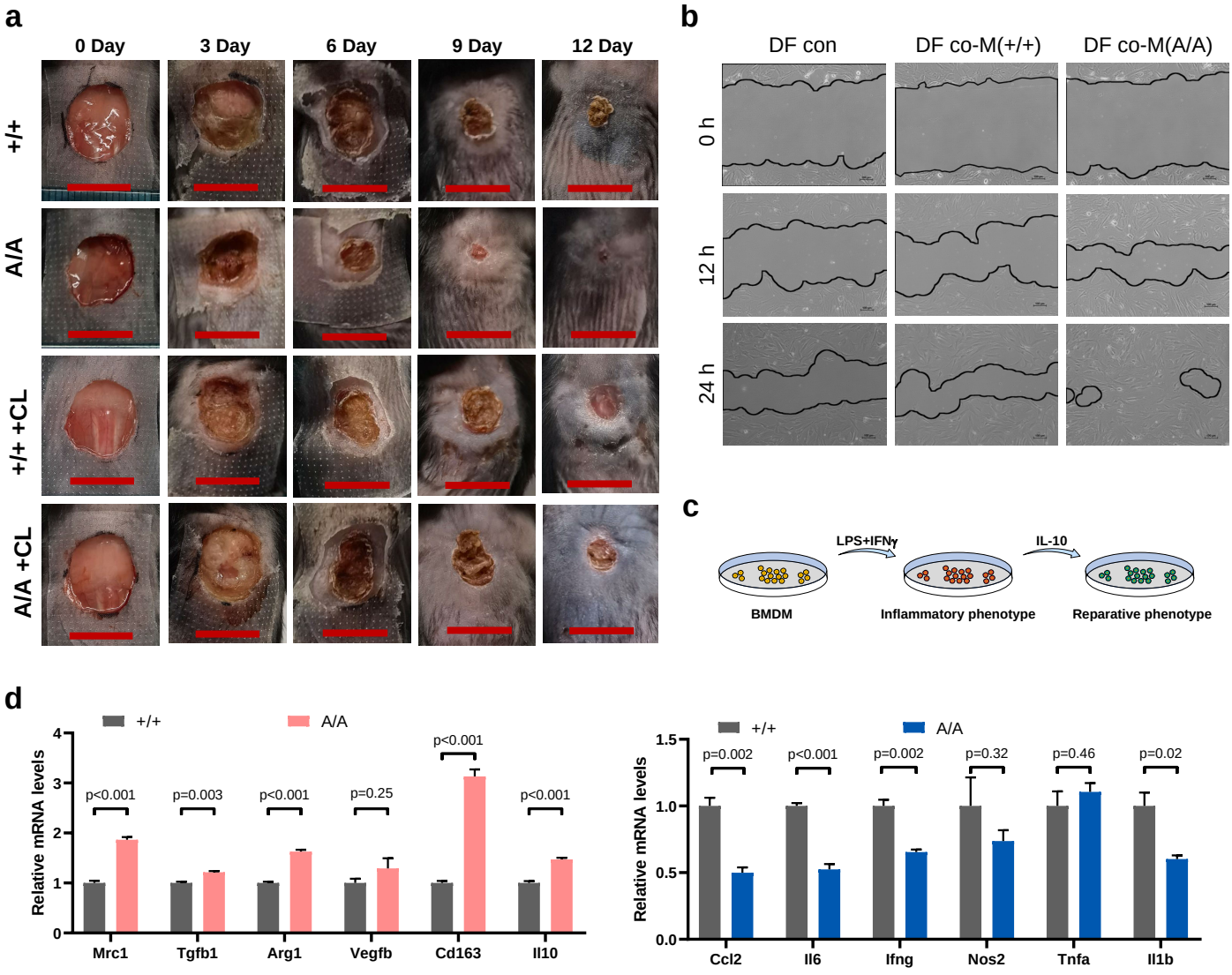

Supplementary Fig. 11 Dephosphorylation of PPARγ T166 mediates the reparative function of macrophages. **a** Representative time-lapse photographs of skin wounds in PPARγ$^{+/+}$ and PPARγ$^{A/A}$ mice after treatment with CL-lipo and Lipo control. **b** Migratory potential ability of DFs co-cultured with PPARγ$^{+/+}$ and PPARγ$^{A/A}$ BMDMs for 24 h. Representative images are shown (Scale bar, 100 μm). Black lines were drawn to mark the original wound at 0 h, and to mark the wound closure resulting from cell movement at 12 and 24 h. **c** BMDMs treated with LPS+IFNγ for 24 h, and then treated with IL-10 for 48 h. **d** Relative mRNA levels of pro-inflammatory and pro-repair associated genes in PPARγ$^{+/+}$ and PPARγ$^{A/A}$ macrophages in response to LPS+IFNγ and IL-10, *n* = 3 biological replicates per group. Data were analysed by a two-tailed Student's *t*-test.

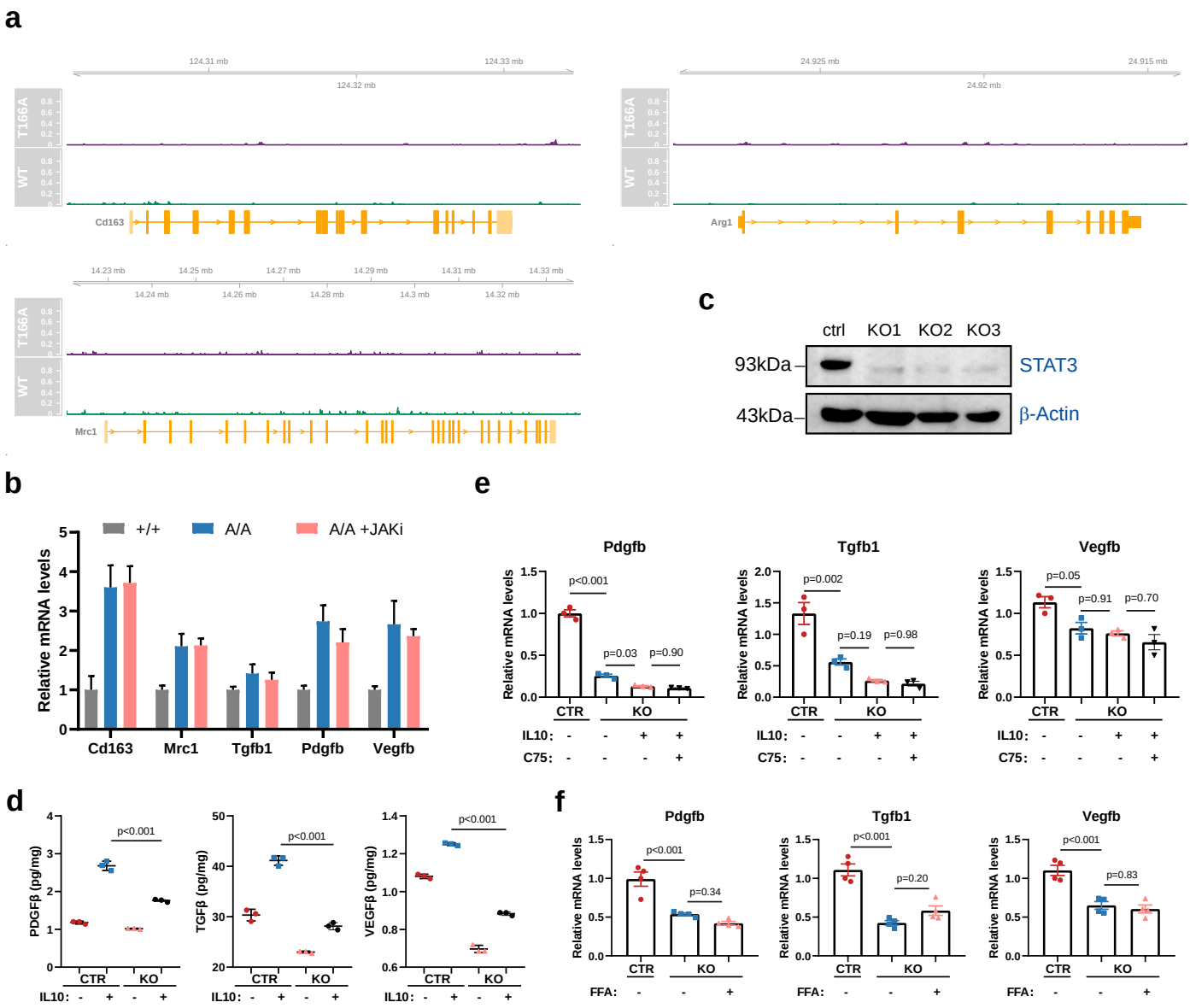

Supplementary Fig. 12 The reparative function of T166A macrophages is independent of JAK activation. **a** Binding peaks of WT or T166A PPARγ around indicated gene region. **b** mRNA expression of the reparative markers *Cd163*, *Mrc1*, *Tgfb1*, *Pdgfb* and *Vegfb* in PPARγ$^{+/+}$ and PPARγ$^{A/A}$ BMDMs treated with JAK1/2 inhibitor Ruxolitinib (10 μM). Data are presented as mean ± s.e.m. of *n* = 3 biological replicates per group. **c** Western blotting analysis of STAT3 expression in STAT3-knockout (KO) RAW264.7 macrophages. **d** The concentration of PDGFβ, TGF-β1 and VEGFβ in STAT3-KO cells in response to IL-10 is determined by ELISA (*n* = 3). Data were analysed by a two-tailed Student's *t*-test. **e** Relative mRNA levels of *Pdgfb*, *Tgfb1* and *Vegfb* in STAT3-KO cells stimulated with C75 in response to IL-10. mRNA amounts normalized relative to *Rplp0* (*n* = 3). Data were analysed by a one-way ANOVA followed by a Tukey's multiple comparisons test. **f** Relative mRNA levels of *Pdgfb*, *Tgfb1* and *Vegfb* in STAT3-KO cells in response to FFAs (100 μM). mRNA amounts normalized relative to *Rplp0* (*n* = 4). Data were analysed by a one-way ANOVA followed by a Tukey's multiple comparisons test.

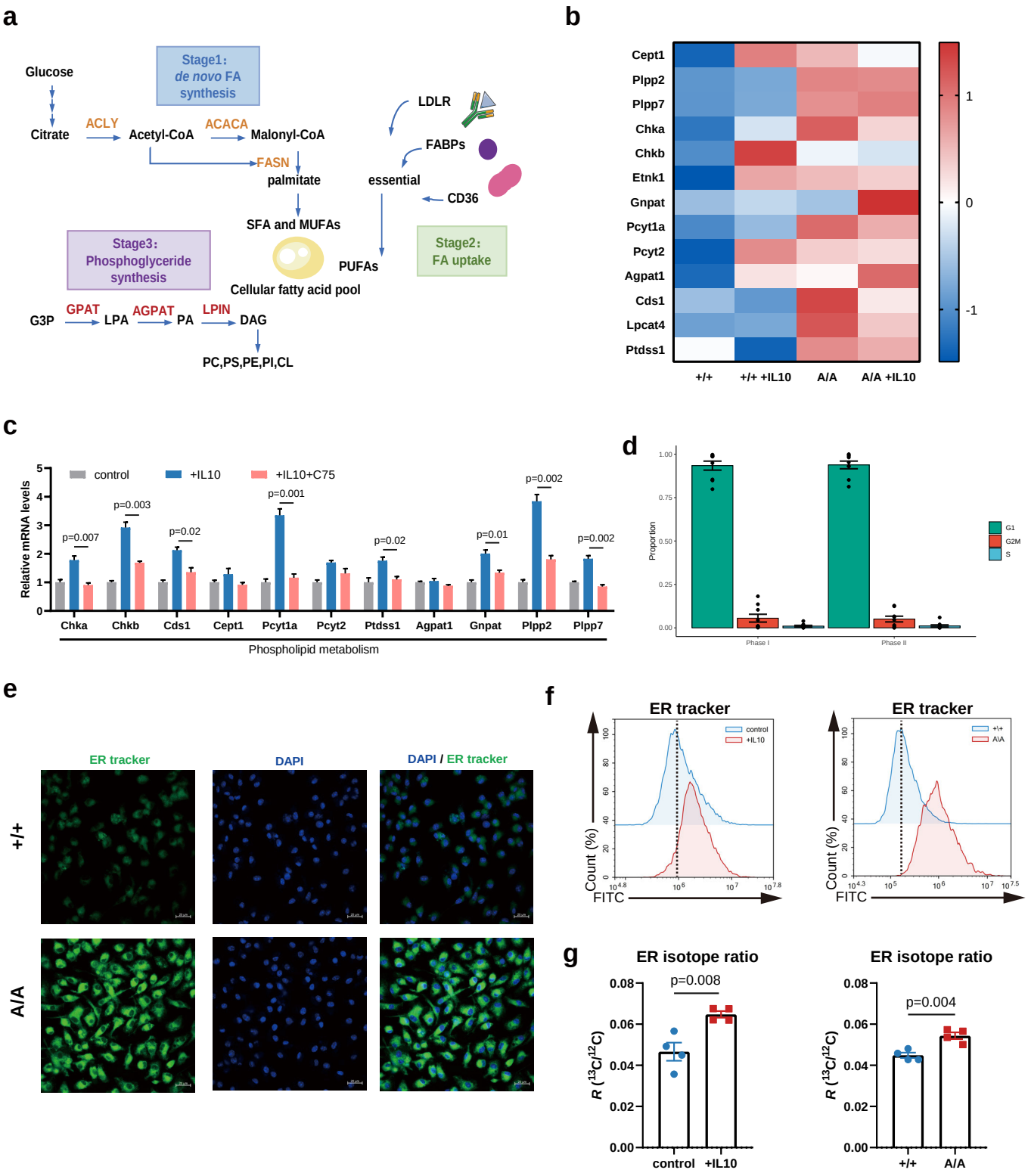

Supplementary Fig. 13 Fatty acids support the expansion of the ER in reparative macrophages. **a** Schematic diagram of phospholipid synthesis. **b** Relative mRNA levels of phospholipid metabolism genes in PPARγ$^{+/+}$ and PPARγ$^{A/A}$ BMDMs stimulated with IL-10 (20 ng/ml) for 48 h, *n* = 3 biological replicates per group. **c** Relative mRNA levels of phospholipid metabolism genes in BMDMs stimulated with C75 in response to IL-10. *n* = 3 biological replicates per group. Data were analysed by a two-tailed Student's *t*-test. **d** Cell cycle analysis of macrophages from phase I and phase II in SKIN scRNA-seq dataset. **e** Representative microscopic images of ER tracker staining in PPARγ$^{+/+}$ and PPARγ$^{A/A}$ BMDMs. Scale bar, 20 μm. **f** Representative flow cytometry plot of ER analysis by ER-tracker fluorescent staining in M(IL10) or in PPARγ$^{+/+}$ and PPARγ$^{A/A}$ BMDMs. **g** The $^{13}C/^{12}C$ isotope ratio of ER from M(IL10) or PPARγ$^{+/+}$ and PPARγ$^{A/A}$ BMDMs. *n* = 4 biological replicates per group. Data were analysed by a two-tailed Student's *t*-test.

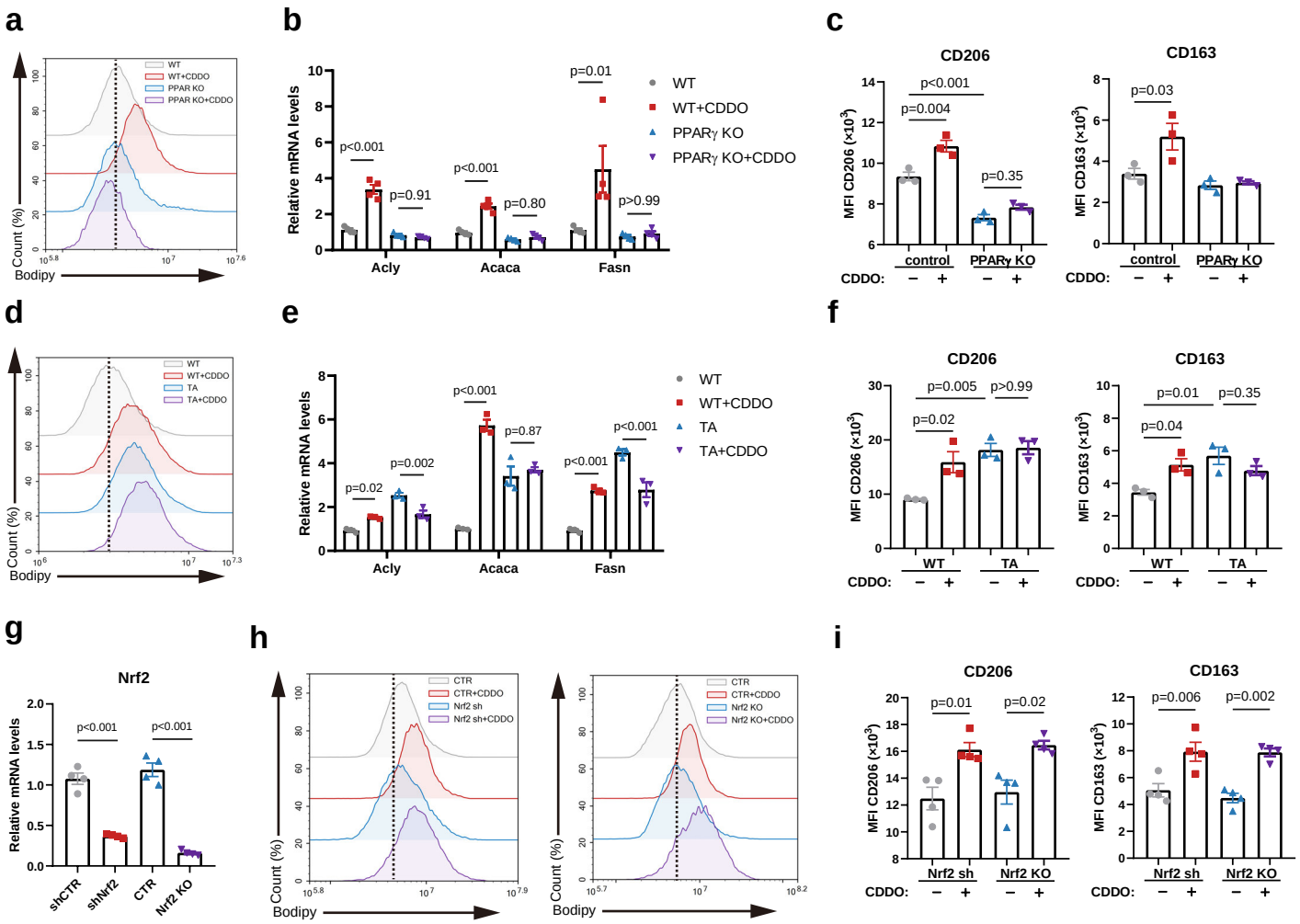

Supplementary Fig. 14 CDDO treatment promotes skin wound healing by inhibiting PPARγ T166 phosphorylation. **a** BODIPY 493/503 staining analysis by flow cytometry in PPARγ-WT or PPARγ-KO RAW 264.7 cells in response to CDDO. **b** Relative mRNA levels of lipid synthesis-related genes in PPARγ-WT or PPARγ-KO RAW 264.7 cells in response to CDDO. *n* = 4 biological replicates per group. Data were analysed by a one-way ANOVA followed by a Tukey's multiple comparisons test. **c** The expression levels of CD163 and CD206 in PPARγ-WT or PPARγ-KO RAW 264.7 cells in response to CDDO were assessed by flow cytometry. Data are mean ± s.e.m. of *n* = 3 biological replicates per group. Data were analysed by a one-way ANOVA followed by a Tukey's multiple comparisons test. **d** BODIPY 493/503 staining analysis by flow cytometry in PPARγ-WT or PPARγ-TA RAW 264.7 cells in response to CDDO. **e** Relative mRNA levels of lipid synthesis-related genes in PPARγ-WT or PPARγ-TA RAW 264.7 cells in response to CDDO. *n* = 3 biological replicates per group. Data were analysed by a one-way ANOVA followed by a Tukey's multiple comparisons test. **f** The expression levels of CD163 and CD206 in PPARγ-WT or PPARγ-TA RAW 264.7 cells in response to CDDO were assessed by flow cytometry. Data are mean ± s.e.m. of *n* = 3 biological replicates per group. Data were analysed by a one-way ANOVA followed by a Tukey's multiple comparisons test. **g** Relative mRNA levels of *Nrf2* (*Nfe2l2*) in shCTR, shNrf2 and Nrf2 KO RAW 264.7 cells. *n* = 4 biological replicates per group. Data were analysed by a two-tailed Student's *t*-test. **h** BODIPY 493/503 staining analysis by flow cytometry in shNrf2 or Nrf2 KO RAW 264.7 cells in response to CDDO. **i** The expression levels of CD163 and CD206 in shNrf2 or Nrf2 KO RAW 264.7 cells in response to CDDO were assessed by flow cytometry. Data are presented as mean ± s.e.m. of *n* = 4 biological replicates per group. Data were analysed by a one-way ANOVA followed by a Tukey's multiple comparisons test.

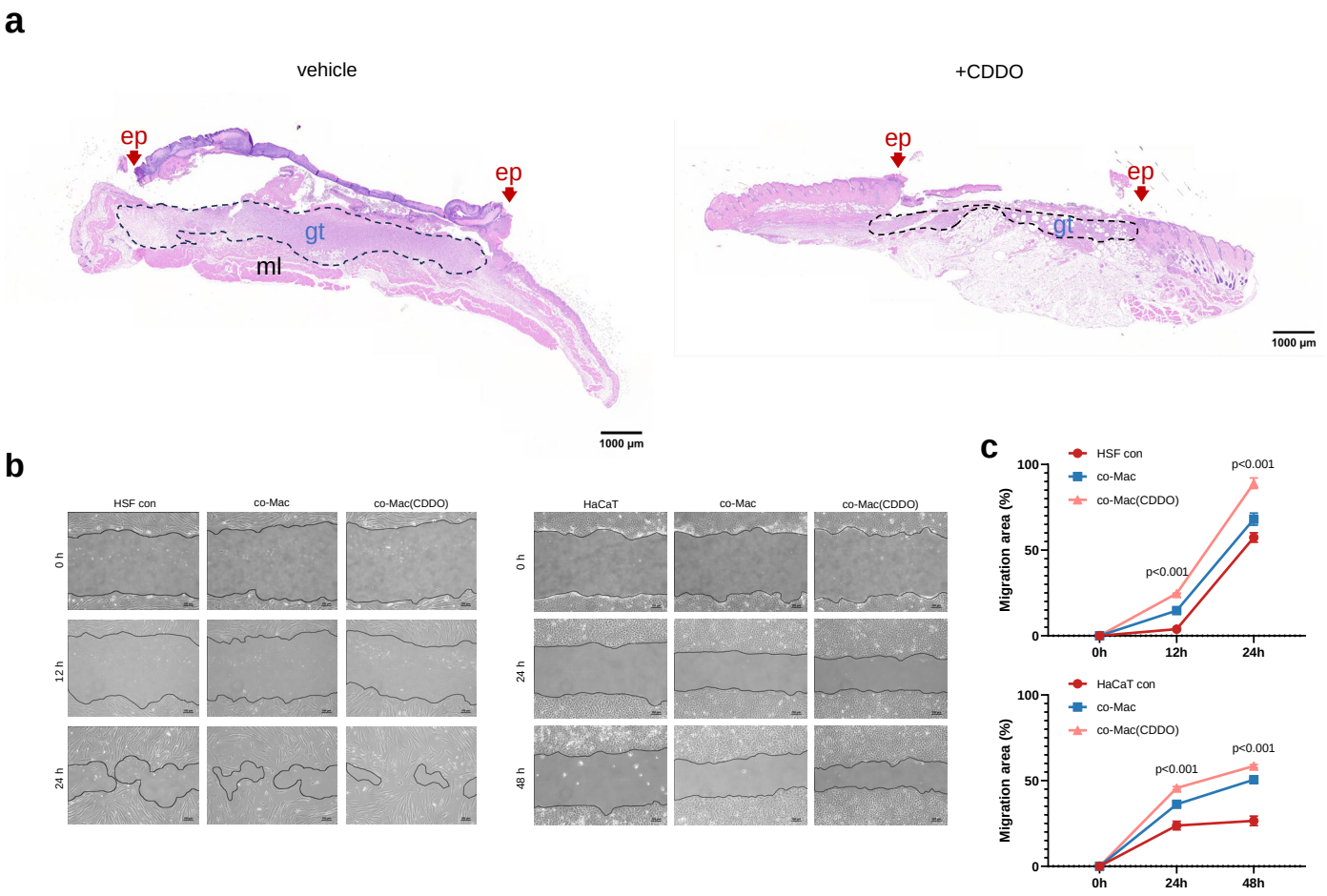

Supplementary Fig. 15 CDDO induces a reparative phenotype in macrophages and accelerates wound healing. **a** Representative H&E images of 6 dpi wound sections from control and CDDO-treated mice. Scale bar, 1000 μm. ep, epidermis; gt, granulation tissue; ml, muscle. Arrows indicate the tips of the epithelial tongues. **b** The scratch wound representative images of HSF and HaCaT cells co-cultured with human macrophages (Mac) or CDDO pretreated Mac with for 48 h. Scale bar, 100 μm. **c** The scratch wound closure rate of HSF and HaCaT cells co-cultured with human Mac or CDDO pretreated Mac (*n* = 3 per group). Data were analysed by a one-way ANOVA followed by a Dunnett's multiple-comparisons test.

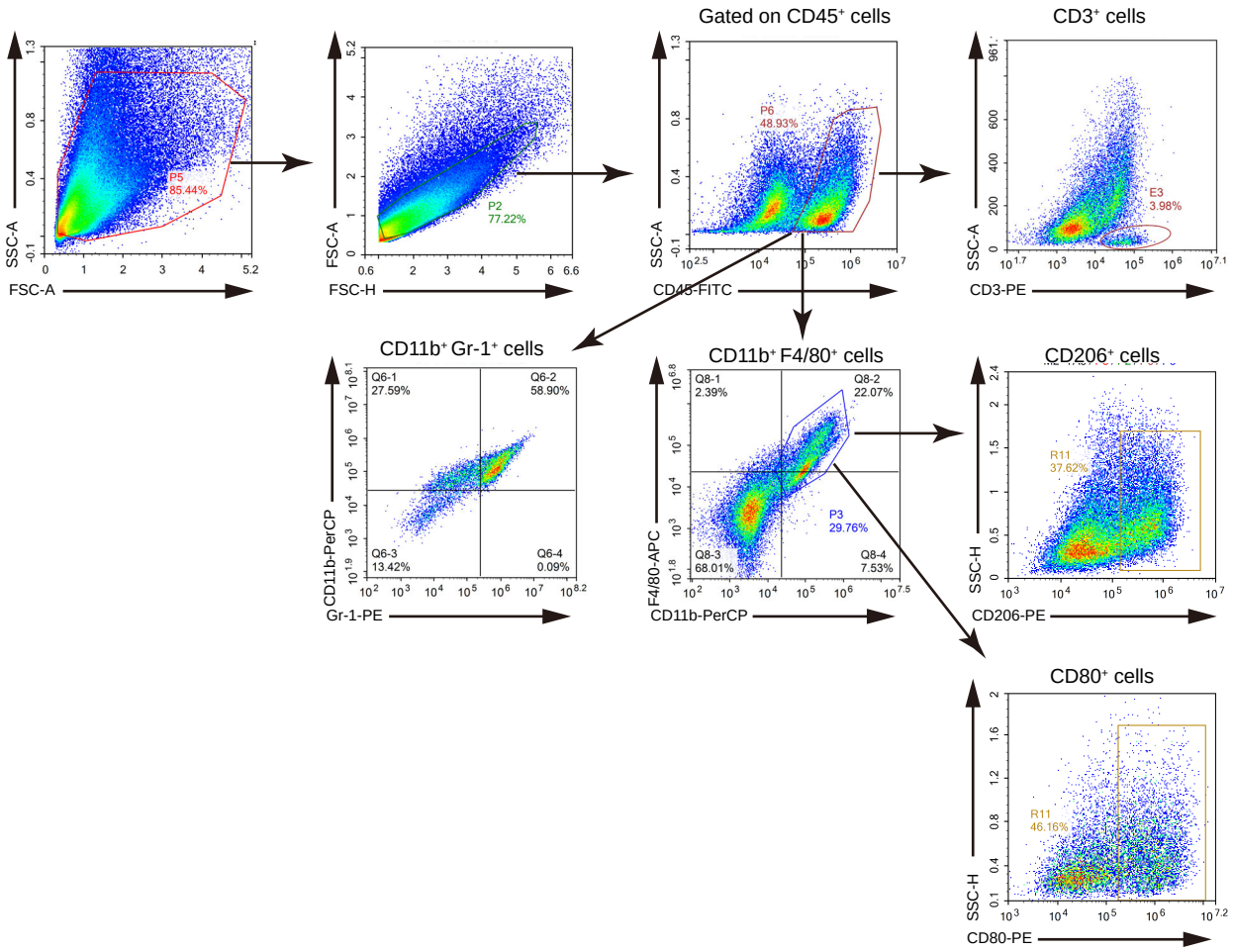

Supplementary Fig. 16 Gating strategy used for the evaluation of immune cell populations in skin wound tissues.

Supplementary Fig. 3d

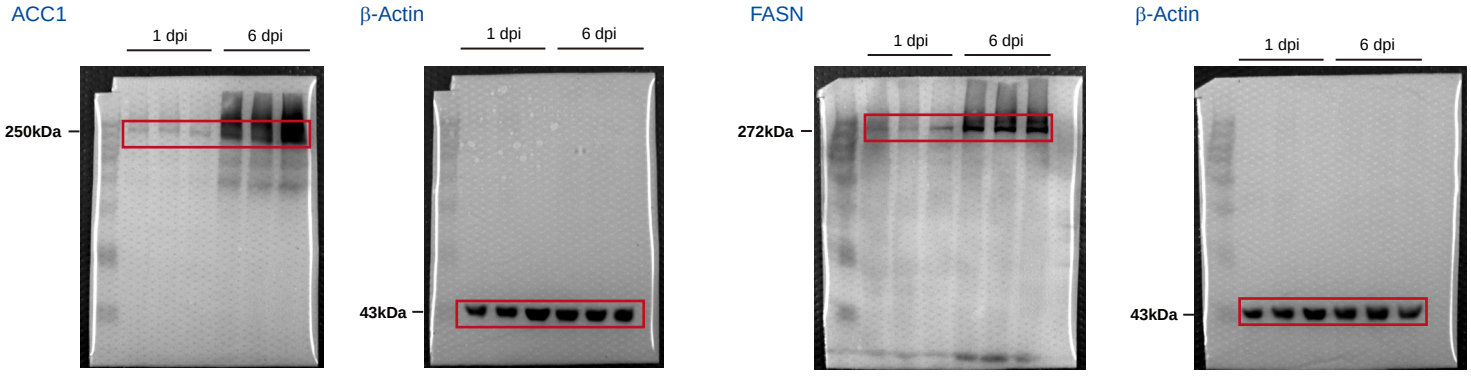

Supplementary Fig. 5b

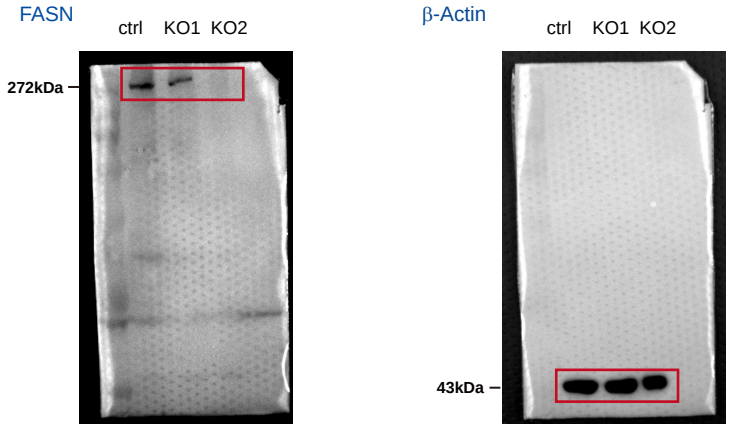

Supplementary Fig. 6c

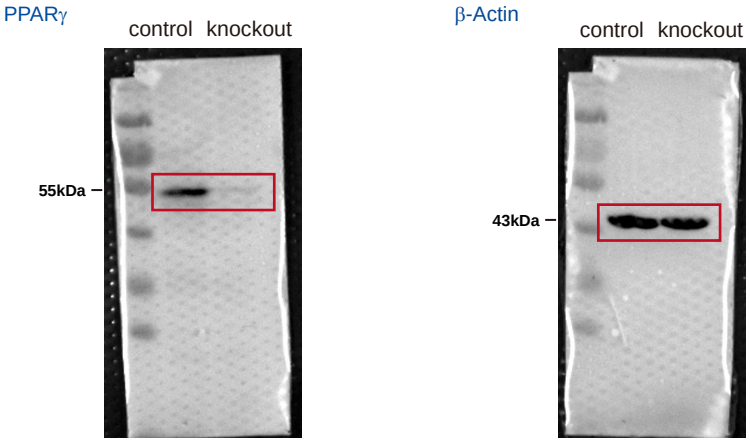

Supplementary Fig. 6f

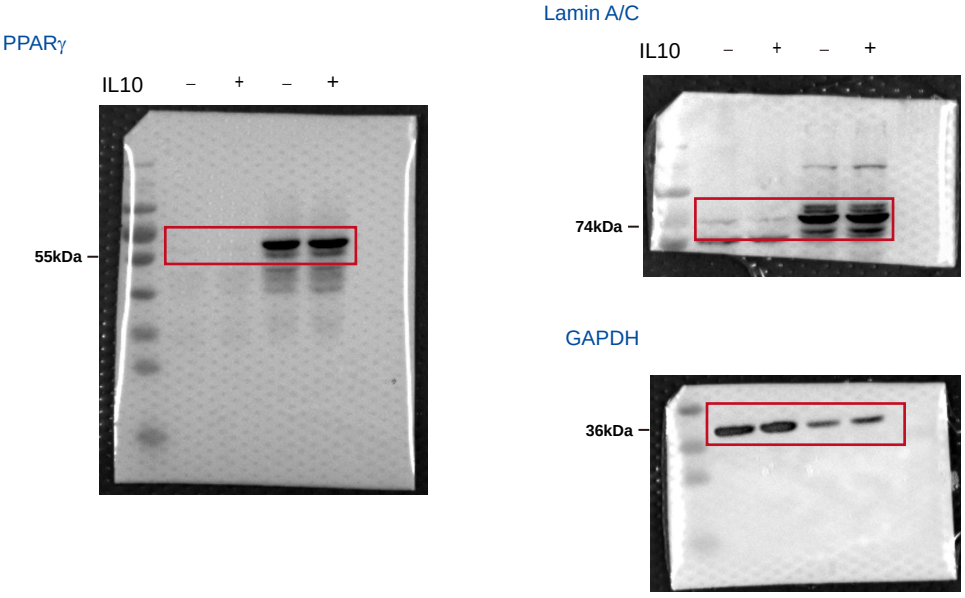

Supplementary Fig. 6g

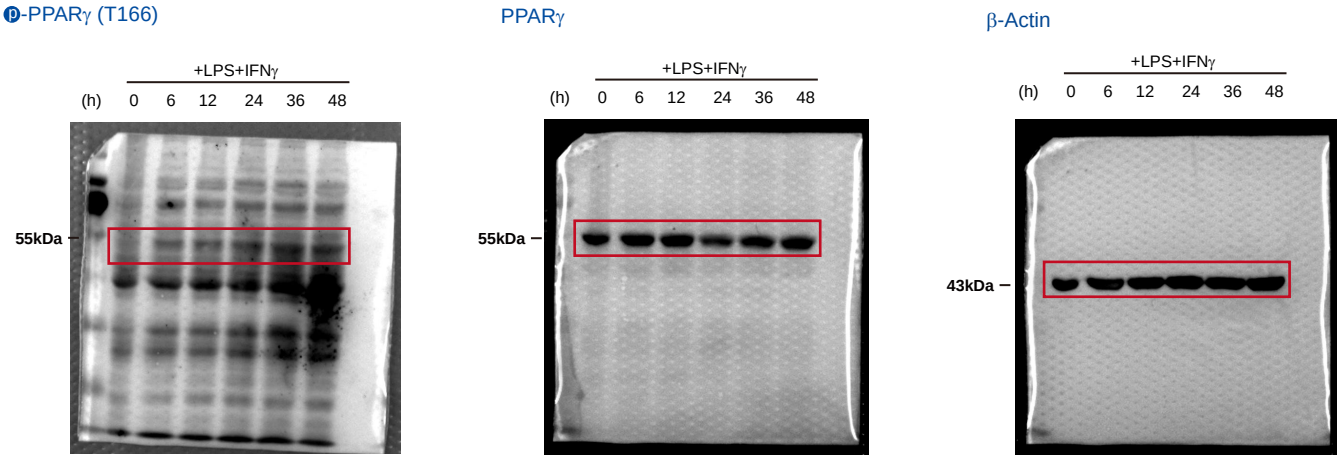

Supplementary Fig. 6h

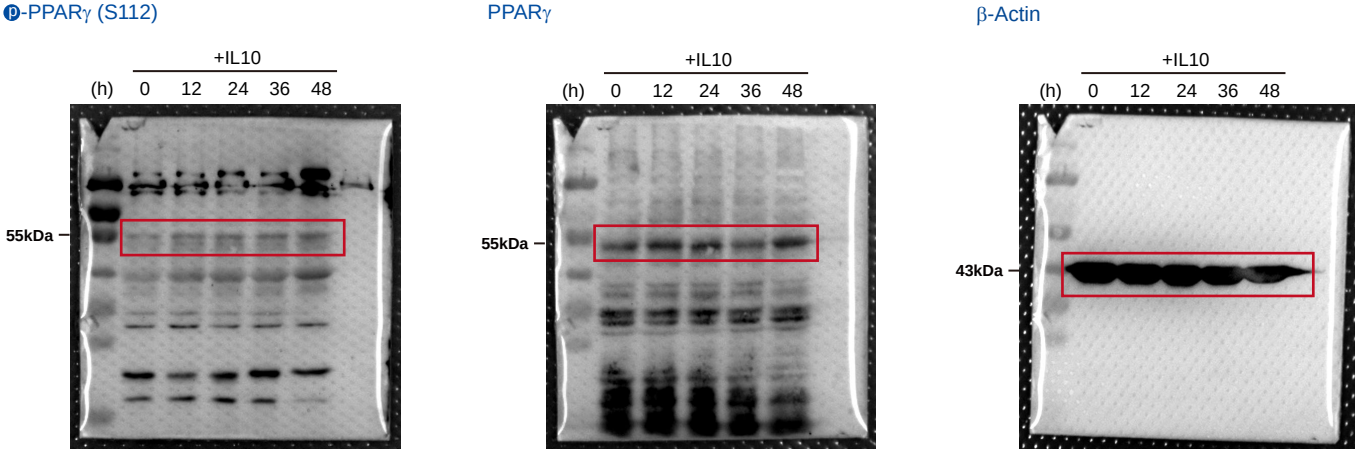

Supplementary Fig. 6h

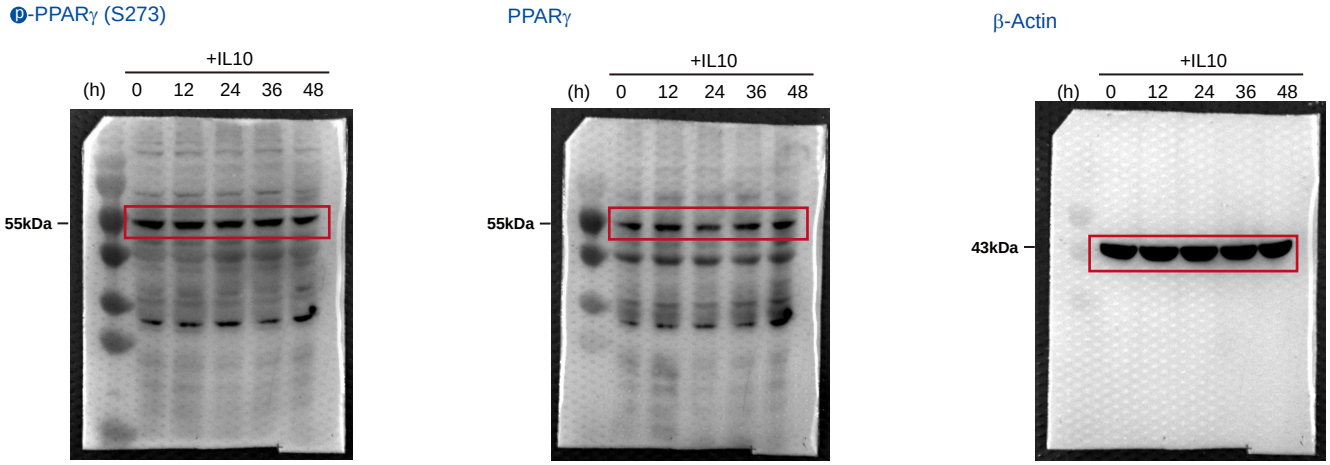

Supplementary Fig. 12c